Design of Ice-free Nanostructured Surfaces Based on Repulsion of Impacting Water Droplets

Lidiya Mishchenko,[†] Benjamin Hatton,[‡] Vaibhav Bahadur,[†] J. Ashley Taylor,[§] Tom Krupenkin,[§] and Joanna Aizenberg[†,‡,*]

[†]School of Engineering and Applied Sciences, [‡]Wyss Institute for Biologically Inspired Engineering, Harvard University, Cambridge, Massachusetts 02138, United States, and [§]Department of Mechanical Engineering, University of Wisconsin-Madison, 1513 University Avenue, Madison, Wisconsin 53706, United States

ABSTRACT Materials that control ice accumulation are important to aircraft efficiency, highway and powerline maintenance, and building construction. Most current deicing systems include either physical or chemical removal of ice, both energy and resource-intensive. A more desirable approach would be to *prevent* ice formation rather than to fight its build-up. Much attention has been given recently to freezing of *static* water droplets resting on supercooled surfaces. Ice accretion, however, begins with the droplet/substrate collision followed by freezing. Here we focus on the behavior of *dynamic* droplets impacting supercooled nano- and microstructured surfaces. Detailed experimental analysis of the temperature-dependent droplet/surface interaction shows that highly ordered superhydrophobic materials can be designed to remain entirely ice-free down to *ca.* −25 to −30 °C, due to their ability to repel impacting water before ice nucleation occurs. Ice accumulated below these temperatures can be easily removed. Factors contributing to droplet retraction, pinning and freezing are addressed by combining classical nucleation theory with heat transfer and wetting dynamics, forming the foundation for the development of rationally designed ice-preventive materials. In particular, we emphasize the potential of hydrophobic polymeric coatings bearing closed-cell surface microstructures for their improved mechanical and pressure stability, amenability to facile replication and large-scale fabrication, and opportunities for greater tuning of their material and chemical properties.

KEYWORDS: anti-icing · superhydrophobic · wetting · dynamic impact · freezing · nanostructured design

Much of the infrastructure required for modern life remains vulnerable to a basic feature of earth's atmosphere: ice. Spread over a surface, even a thin ice layer is enough to bring down power lines, burst pipes, make roads impassable, and, as most recently demonstrated by the tragic crash of Flight 3407 in Buffalo, cause dangerous loss of lift force by aircraft wings.[1] Accumulated ice is so sturdy that large-scale breaking is difficult if not impossible: even the "pneumatic boot", a rubber coat on plane surfaces designed to crack ice by inflating, is no match for severe ice. Melting is the common alternative way to mitigate ice threats, but both thermal and chemical methods are plagued by problems. Continuous heat guzzles energy, while selective heating relies on fallible detection and activation techniques that introduce serious risk. Salts lower the freezing point but corrode surfaces and disrupt osmotic balance in the environment, and glycols deplete oxygen in streams and lakes. Particularly on planes, chemical release timing often depends on the same fallible judgment as selective heating. Chemicals can alternatively be incorporated into protective coatings, but since by nature they have to dissolve in incipient ice to work, they wash away and must be monitored and replaced frequently. Currently we have no sustainable technology for dealing with ice; the methods we have are resource-intensive, toxic, and/or not reliably up to the task.

For ice formation associated with droplet impact on a surface, the ability to fend off water droplets could lead to prevention of icing as an inherent material property. This completely different approach to tackling ice buildup is inspired by the technology used by many organisms to manipulate water droplets on their surfaces. From mosquitoes defogging their eyes[2] to water striders keeping their legs dry,[3] the common theme is a superhydrophobic surface (SHS),[4−6] which repels water not only chemically but also geometrically *via* an array of nanoscale bristles that determine the reduced surface area a droplet encounters. Here we propose and test a hypothesis that the reduced surface contact time and contact area of impinging water droplets on properly designed SHS can leave the surface ice-free if the droplets bounce off before ice nucleation can occur.

Although the manipulation of aqueous phase transitions (condensation[7] and freezing[8,9]) *via* surface chemistry has been explored for quite some time and much

See the accompanying Perspective by Meuler *et al.* on p 7048.

*Address correspondence to jaiz@seas.harvard.edu.

Received for review September 28, 2010 and accepted October 28, 2010.

Published online November 9, 2010. 10.1021/nn102557p

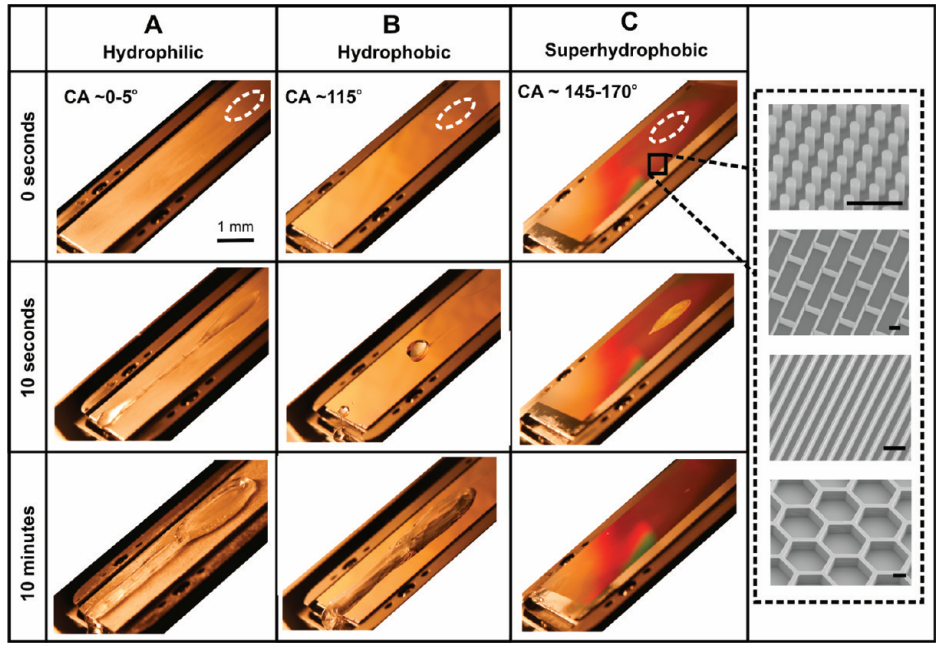

Figure 1. Ice accumulation on flat aluminum (A), smooth fluorinated Si (B), and microstructured fluorinated Si (C) surfaces. The advancing contact angle (CA) of the water droplets on these surfaces is indicated. Insets show micrographs of exemplary superhydrophobic surfaces: posts, bricks, blades, and honeycombs (scale bars: 10 μm). A stream of droplets ($T_{droplet}$ = 0 °C) was impinged from a 10 cm height at a rate of 0.06 mL/sec onto the surfaces ($T_{substrate}$ = −10 °C) tilted at 30°. White dashed circles indicate the position of droplet impact. Ice accumulation was observed on both hydrophilic and hydrophobic surfaces, while no freezing or accumulation was observed on the superhydrophobic surface even after a significant period of time.

attention has been given recently to the interaction of *static* droplets with a SHS,[10−15] the analysis and understanding of the wetting behavior of *dynamic* droplets impacting these surfaces are severely limited and mostly cover room temperature or elevated temperature conditions.[16−19] It has been proposed that at room temperature, a droplet bouncing off a SHS behaves similarly to a harmonic spring as it impacts, spreads, and retracts from the surface.[17] The influence of reduced temperatures on this behavior is not entirely obvious and has not been studied. Although the icephobic potential of a SHS has been discussed recently, the studies mainly focused on the analysis of freezing of static droplets or streams of water, with consideration limited to the ability of a SHS to weaken ice adhesion[20,21] and delay ice nucleation.[22−24] The current work puts emphasis on the critical questions about the behavior of *dynamic* supercooled droplets impacting a surface as a function of substrate temperature, the underlying mechanism of freezing on such nano/microstructured superhydrophobic surfaces, and ultimately, the parameters that are crucial in designing anti-icing materials.

RESULTS AND DISCUSSION

To address our questions about the dynamic interaction of water droplets with cooled superhydrophobic surfaces, we have fabricated Si substrates bearing high-aspect-ratio, ordered surface structures of various geometries and feature sizes (Figure 1 inset). The feature sizes and the corresponding solid fractions (so-called phi-ratio) of the exemplary SHS are summarized in Table 1. These engineered, ordered substrates are ideal as model systems for studying potential anti-icing applications, allowing for precise control and analysis of the parameters. When a hydrophobic coating is applied, these surfaces demonstrate remarkable superhydrophobicity (see Table 2 for wetting properties).[10−15] After fabrication and surface treatment, we performed a series of dynamic droplet experiments at freezing conditions comparing the performance of structured superhydrophobic substrates with that of flat hydrophobic, and hydrophilic surfaces. Water droplets (~15 μL, $T_{droplet}$ = −5 to 60 °C) were impinged from a 10 cm height onto substrates ($T_{substrate}$ = 20 to −35 °C) positioned at various tilt angles (0°, 30°, 60°) under low humidity conditions (see Methods for details).

TABLE 1. Geometrical Parameters of Structured Surfaces

	features (μm)			
sample	pitch	height	wall/post thickness	ϕ-ratio
staggered bricks	38.5 15.4	10.9	1.4	0.1
posts	3.6	9.9	1.5	0.1
posts (wide)	16.2	7.8	4.5	0.1
blades	5.2	6.0	1.0	0.2
honeycombs	34.5	7.5	3.3	0.4

TABLE 2. Advancing and Receding Contact Angles of Most Commonly Used Surfaces

	contact angles	
sample	advancing	receding
staggered bricks	158 ± 6	118 ± 6
posts	165 ± 4	133 ± 3
posts (wide)	170 ± 3	
flat silicon (hydrophobic)	114 ± 6	86 ± 5

The substrates—rough aluminum, smooth fluorinated silicon, and various superhydrophobic surfaces—were first tested for their ability to accumulate ice over extended periods of time at freezing temperatures (Figure 1). A stream of droplets ($T_{droplet}$ = 0 °C) was impinged from a 10 cm height at a rate of 0.06 mL/sec onto the surfaces ($T_{substrate}$ = −10 °C) tilted at 30°. While the flat hydrophobic surface showed a ~1 min delay in ice formation as compared to the hydrophilic surface, significant ice accumulation did occur over a 10 min span for both substrates (Figure 1A,B). The latter observation suggests that surface chemistry alone is of limited use in ice-*prevention* technologies, as it would delay but not avoid ice buildup. The SHS, on the other hand, is a promising alternative, as no ice accumulation was observed after 10 min of water flow (Figure 1C). Note that the small amount of condensation occurring on the SHS, seen in Figure 1C as a bright spot on the substrate at 10 s, did not affect its anti-icing properties. This ice-repellent behavior was characteristic of many SHSs with varying geometry (Figure 1C inset), position, and substrate and droplet temperatures.

To understand the mechanisms by which an SHS prevents ice accumulation, we analyzed the behavior of single droplets impinging upon the same three substrates at $T < 0$ °C from a 10 cm height. A high-speed videocamera was used to capture sequential images of droplet impact, maximum spreading (r_{max}), maximum retraction (r_{min}), and freezing. Both tilted (Figure 2) and horizontal (Figure 3) substrates showed the same characteristic features: (A) on high-friction hydrophilic Al surfaces, the retraction after the spreading was negligible, $r_{min} \approx r_{max}$, leading to large-area surface contact and effective freezing of the droplet (within seconds for $T_{substrate} < -10$ °C); (B) while droplets underwent significant retraction on smooth hydrophobic Si surfaces, they remained pinned and did not fully withdraw, $r_{min} > 0$, resulting in freezing for any $T_{substrate} < 0$ °C (freezing within seconds for $T_{substrate} < -10$ °C); (C) on the superhydrophobic surfaces, complete retraction occurred, $r_{min} = 0$, at $T_{substrate} > -25$ to −30 °C (see Supporting Information, video 1). In other words, the droplets bounce off superhydrophobic surfaces before nucleation takes place, preventing droplet freezing even at supercooled substrate temperatures.

These results suggest that the design of nano- and microstructured materials that induce complete retraction of impacting water droplets before ice nucleation occurs may prove to be an effective strategy to prevent ice formation. To explore the full potential of this property, we performed a systematic study of the retraction behavior of droplets impacting a hydrophobic surface and a SHS for various combinations of droplet/substrate temperatures. The radii of the droplets in contact with the substrate were measured from consecutive images taken at 2 ms intervals, and the reduction in the normalized droplet−substrate contact area of the retracting droplets, $R^2 = \pi r^2/(\pi r_{max}^2)$, was plotted as a function of time.

Figure 4A shows exemplary plots depicting the time evolution of R^2 for supercooled droplets ($T_{droplet}$ = −5 °C) as they withdraw from the substrates at $T_{substrate}$ = 20, −15, and −25 °C. On our hydrophobic substrates (blue curves), all droplets pin and remain in place, and those on cold substrates eventually freeze. Our data

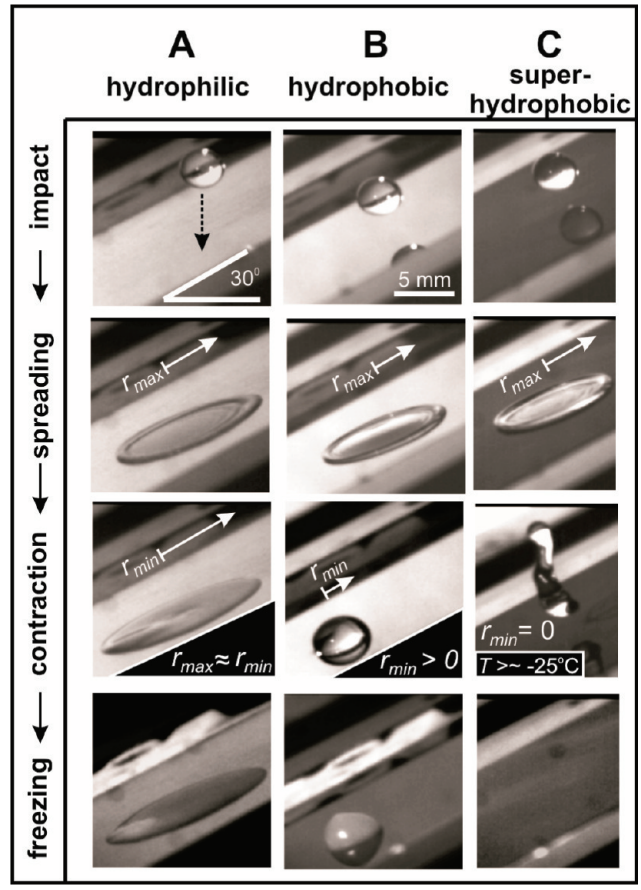

Figure 2. Dynamic behavior of single droplets (~15 μL volume) impinging upon 30° tilted surfaces at $T_{substrate} < 0$ °C from a 10 cm height. Images from top to bottom depict droplet impact, maximum spreading (r_{max}), maximum retraction (r_{min}), and freezing. On hydrophilic Al surfaces (A) and hydrophobic Si surfaces (B), the droplets failed to retract entirely after spreading ($r_{min} > 0$), remained in contact with the substrates and froze for any $T_{substrate} < 0$ (freezing within seconds for $T_{substrate} < -10$ °C); while on the SHS (C), they fully retracted and bounced off the surface leaving no residue at $T_{substrate} > -25$ to −30 °C.

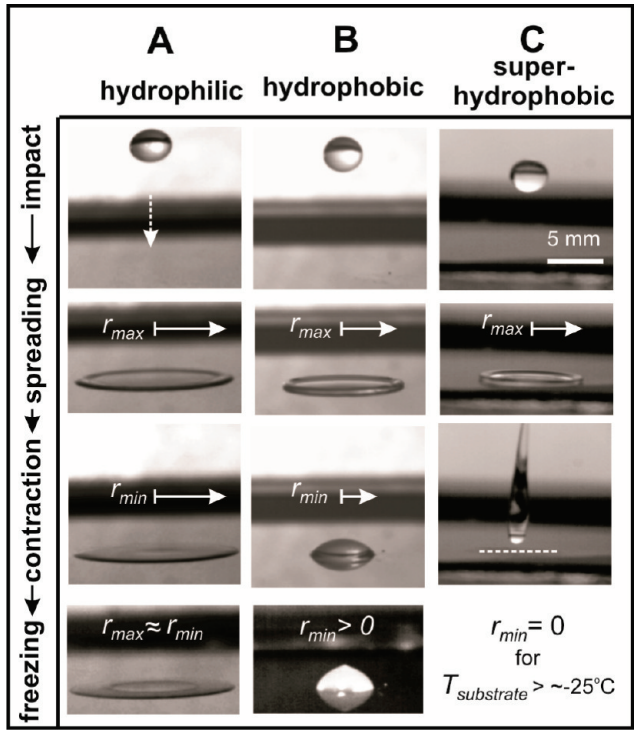

Figure 3. Sequential images of the dynamic behavior of ~15 μL droplets impacting cooled ($T_{substrate} < 0$ °C) horizontal surfaces from a 10 cm height. Images from top to bottom depict droplet impact, maximum spreading (r_{max}), maximum retraction (r_{min}), and freezing. Pinning and ice formation were observed on hydrophilic (A) and smooth hydrophobic (B) surfaces, while full retraction was observed on the superhydrophobic surfaces (C).

provide the first experimental evidence that with decreasing substrate temperatures, impacting droplets on flat surfaces undergo a significant reduction in retraction speed and decrease in maximum retraction height, *H*, before pinning (Figure 4B, top), apparently due to energy losses resulting from increased viscous shear and dissipation at the three-phase contact line. On the SHS (red curves), droplets behave as if on a frictionless surface, following the same curve independently of substrate or droplet temperature for a wide temperature range ($T_{droplet} = +60$ to -5 °C, $T_{substrate} = 20$ °C to -25 to -30 °C, not all curves shown). On these surfaces, for $T_{substrate} > -25$ °C, droplets fully retract and leave the surface within ~20 ms. Below this approximate temperature, a pinning transition occurs, and droplets remain in contact with the SHS and freeze (Figure 4B, bottom).

We observed under our experimental conditions that, even upon impact, the droplets that freeze on the SHS below the transition temperature remain in a nonwetting Cassie state similar to static droplet freezing,[21] making ice buildup much more tractable than the stubborn sheets formed on flat surfaces. To demonstrate this new and important observation, a group of droplets ($T_{droplet} = 20$ °C) was impinged from a 10 cm height simultaneously onto three surfaces ($T_{substrate} = -30$ °C) tilted at 15°, freezing immediately upon contact. With a small thermal energy input, as the substrate temperature was raised above 0 °C, layers of ice which formed on the patterned superhydrophobic region easily slid off, pinning only at the unpatterned hydrophobic regions (Figure 5). Moreover, while frozen droplets can be removed from the SHS in their entirety, the adhesion of ice on smooth, hydrophobic silicon surfaces in our experiments is so strong, that attempts to detach the frozen droplet resulted in fracture and incomplete removal (Supporting Information, video 2).

The temperature-induced pinning transition of droplets observed for the SHS below -25 to -30 °C can be explained using a multiphysics model which analyzes droplet impact dynamics, heat transfer, and heterogeneous ice nucleation at the interface between the droplet and the nanostructure (Figure 6). The retraction of droplets (droplet dynamics) is caused by surface tension. For an ideal frictionless surface, the quasi-harmonic[17] velocity-independent behavior and position

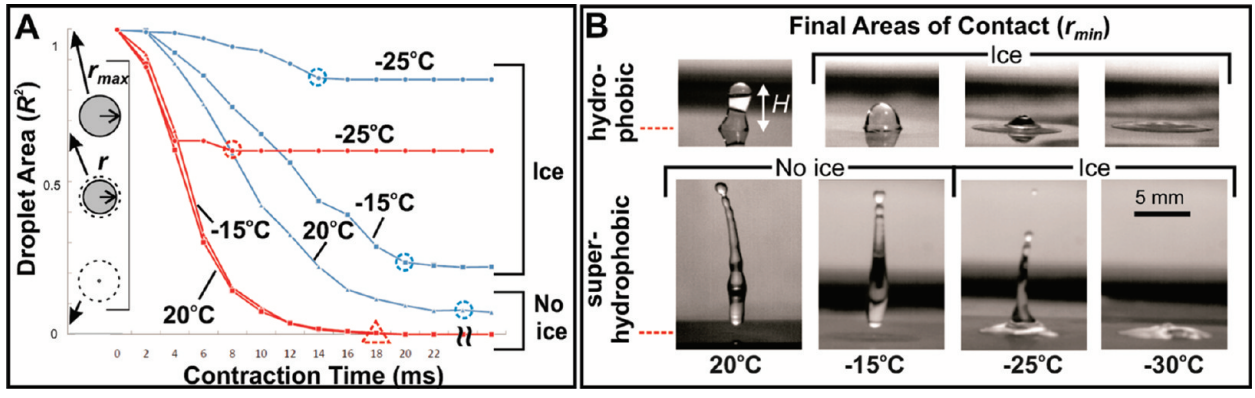

Figure 4. Dynamic retraction behavior of supercooled (−5 °C) droplets (~15 μL volume) as a function of substrate temperature. (A) Reduction in the normalized droplet-substrate contact area, $R^2 = \pi r^2/(\pi r_{max}^2)$, measured from consecutive images taken at 2 ms intervals for droplets retracting on superhydrophobic (red) and hydrophobic (blue) surfaces of different temperatures ($T_{substrate}$ is indicated next to the plots). Dashed circles indicate pinning of the contact line at the surface. The dashed triangle labels a complete droplet retraction and repulsion from the surface. Freezing will occur for any droplets that have not left a cooled surface. (B) Still images depicting droplets, dropped from a 10 cm height, at maximum retraction (r_{min}) for each substrate temperature (dashed lines indicate surface level). Note the gradual increase of r_{min} and decrease of droplet height, *H*, at maximum retraction on the flat surface (top), and the sudden pinning transition on the superhydrophobic surface (bottom) upon decrease of the surface temperature.

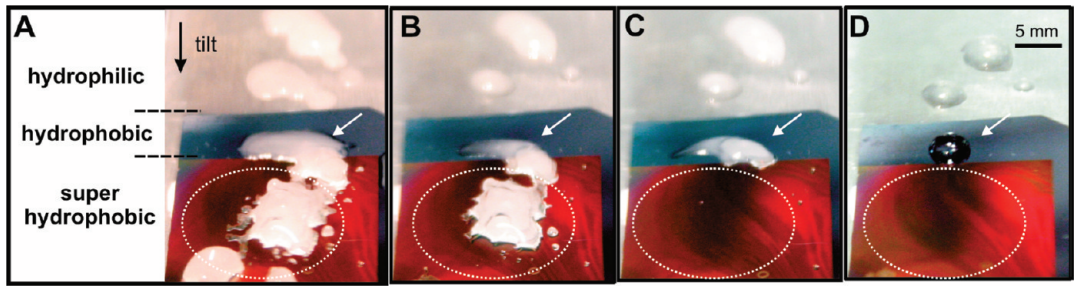

Figure 5. Sequential images of ice layer removal from hydrophilic Al, fluorinated hydrophobic Si, and microstructured fluorinated Si (SHS). A group of droplets ($T_{droplet}$ = 20 °C) was impinged from a 10 cm height simultaneously onto three surfaces ($T_{substrate}$ = −30 °C) tilted at 15°, freezing immediately upon contact (A). As the substrate temperature was raised above 0 °C, the droplets on the SHS that were not in contact with those pinned at the unpatterned hydrophobic region (see droplets located at the bottom of the imaged area) immediately slid off (B), followed by the removal of the droplets on SHS that were bridged with the droplets frozen on the unpatterned hydrophobic region (C) (shown with a dashed oval); while droplets on the unpatterned hydrophobic region (indicated with a white arrow) and the hydrophilic region remained pinned even upon fully melting (D). This indicates that even below the transition temperature, droplets are able to stay nonwetting on a SHS upon impact.

R of the droplets vary predictably as a function of time. By examining the force balance at the contact line, and assuming that the mass of the droplet is localized at its periphery, we derive an equation for this behavior:

$$\frac{d^2R}{dt^2} + \frac{1}{2}(1 - \cos\theta)R = 0 \qquad (1)$$

where R is dimensionless position of the contact line; θ is the receding contact angle, and t is dimensionless retraction time normalized by a characteristic time constant (Figure 6A). The second term in this equation, which is proportional to R, represents the influence of the "retraction" force $F(\theta)$, which is analogous to the spring constant in the classical harmonic oscillator representation. The "retraction" force $F(\theta)$ depends on the receding contact angle θ of water on the structured surface.

During the contact time interval, the heat transfer from a warmer droplet to the cold substrate through the nanostructure and the air gaps (Figure 6B) determines the interfacial temperature. Using a simplified 1D heat conduction model, we can derive an equation for the transient temperature of the water at the interface, $T_{interface}$:

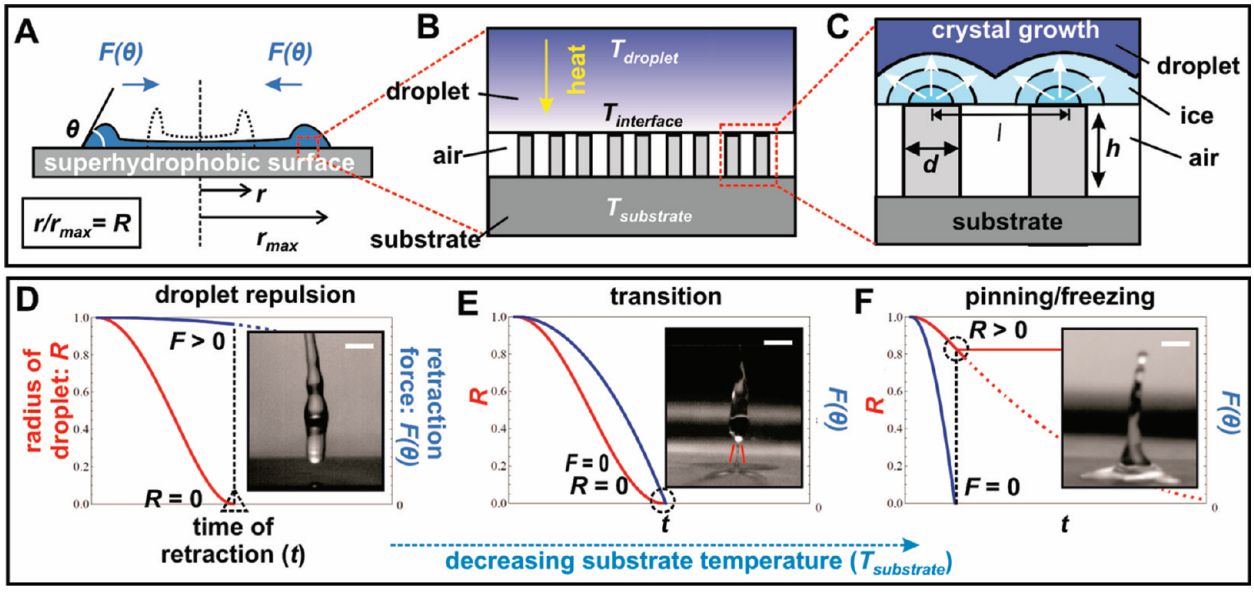

Figure 6. Modeling of droplet freezing on superhydrophobic surfaces using classical heterogeneous nucleation theory and analysis of dynamic wetting behavior. (A) A schematic of a retracting droplet. The retraction force $F(\theta)$ pulling the droplet toward the center originates from surface tension and depends on receding contact angle θ. (B) A schematic showing heat transfer from the droplet to the colder substrate, through the nanostructures and the air gaps. (C) A schematic showing hemispherical ice caps nucleated on the post tips, which reduce the dynamic contact angle. (D−F) Plots of the theoretical normalized radius (position) of the droplet (red), R, during contraction and the retraction force $F(\theta)$ acting on the droplet (blue) for three different substrate temperatures. These plots illustrate the model's predictive powers: if the retraction force is positive when $R = 0$, the droplet fully retracts and bounces off the surface completely (D); the critical pinning transition occurs when the retraction force becomes zero at the time when $R = 0$ (E); when the retraction force reaches zero before the droplet fully retracts, the contact line pins at that location and the droplet eventually freezes (F). Insets show the corresponding experimental images (scale bars are 2 mm). Red lines in panel E highlight the small remaining capillary bridge between the droplet and the substrate at the pinning transition.

$$T_{interface}(t_c) = \\ = T_{droplet} + (T_{substrate} - T_{droplet})\frac{\mathrm{erfc}\left(\frac{h}{2\sqrt{\alpha_{ns}t_c}}\right)}{\mathrm{erfc}\left(\frac{h}{2\sqrt{\alpha_w t_c}}\right)} \quad (2)$$

where erfc denotes the complementary error function, $T_{interface}(t_c)$ is the droplet−substrate interface temperature, $T_{droplet}$ is the initial droplet temperature, $T_{substrate}$ is the temperature at the base of the substrate, h is the height of the raised features, t_c is the total time of contact of liquid at a particular radial position (spreading and retraction), and α_{ns} and α_w are the thermal diffusivities of the structured substrate (volume averaged properties of silicon and air) and water, respectively. The resulting equation elucidates, using typical experimental values, that $T_{interface}$ is strongly dominated by $T_{substrate}$, and not the initial $T_{droplet}$. This has been confirmed experimentally for $T_{droplet} = -5$ to $+60$ °C, where the freezing transition of all the droplets was observed to occur at approximately the same substrate temperature, between -25 and -30 °C. Since the diffusivity of air is similar in magnitude to that of silicon, there is also very rapid equilibration compared to the residence time of the droplet on the surface. Thus, only large (orders of magnitude) changes in structure height would impact $T_{interface}$ (and therefore ice nucleation) significantly.

The interfacial temperature determines the probability and rate of growth of ice crystals and can be predicted by classical heterogeneous nucleation theory. When ice grows on the tips of the posts (Figure 6C), the receding contact angle of the water on the structured surface decreases, due to the increasing hydrophilicity and areal density of features (ϕ) in contact with the droplet. These changes in contact angle strongly affect the contact angle-dependent retraction force acting on the droplet, reducing the droplet's ability to contract fully. Thus, by combining wetting dynamics, thermal transport, and nucleation theory, one can relate the retraction force (in eq 1) to the interfacial temperature, time of contact, and the geometry of the surface structures to predict the behavior of the droplet as a function of time for different substrate temperatures:

$$\frac{d^2R}{dt^2} + (1 - C\phi_0 e^{f(T_{interface})t_c^2})R = 0 \quad (3)$$

where C incorporates empirical and theoretical constants, f is a function of the interface temperature, $f(T_{interface}) \approx -T_{slf}^2/((T_{slf} - T_{interface})^2 T_{interface})$ (T_{slf} being the temperature of the freezing front, 0 °C), and ϕ_0 is the initial ϕ-ratio of the structure without any ice. The exponential dependence of the retraction force on interfacial temperature in the model explains why the observed behavior on the SHS suddenly changes significantly over a narrow temperature range. These results imply that for substrate temperatures above the transition temperature, even if a droplet experiences several impacts before leaving a tilted surface, it will not freeze. (A more detailed description of the model will be reported elsewhere.)

Using eq 3, one can numerically plot, as shown in Figure 6D−F, both the position of the droplet (R, red curves) and the retraction force ($F(\theta)$, blue curves) as a function of time for different substrate temperatures to predict the transition temperature. For successful and complete droplet repulsion, it is essential that the retraction force remain positive throughout the retraction process (until $R = 0$); this is seen at high substrate temperatures (Figure 6D). Figure 6E corresponds to the

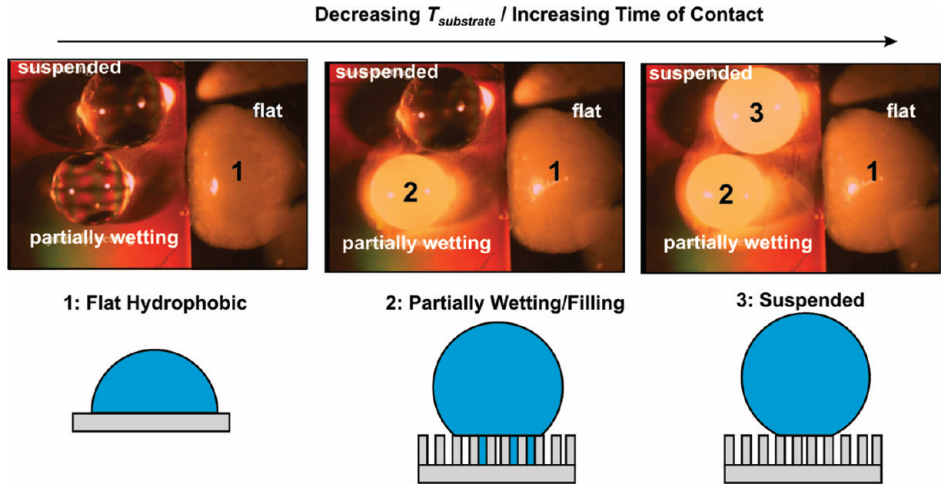

Figure 7. Freezing of static droplets on smooth hydrophobic and superhydrophobic silicon. The droplets were placed on the same fluorinated Si substrate at the interface between the flat and nanostructured regions. The temperature of the substrate was gradually decreased from 0 to −20 °C at a rate of −5 °C/min. We observed a significant delay in freezing of a nonwetting, suspended (Cassie) droplet on the SHS region (3), as compared to a droplet on the flat hydrophobic region (1) and to a partially wetting (partial Wenzel) droplet on the SHS region (2) (induced to collapse using electrowetting), presumably due to differences in heat transfer from the surface to the droplet. All three droplets froze under the same substrate temperature (±1 °C), with a 16 s time delay between freezing events of 1 and 3. Snapshots are 11 × 8 mm² in area.

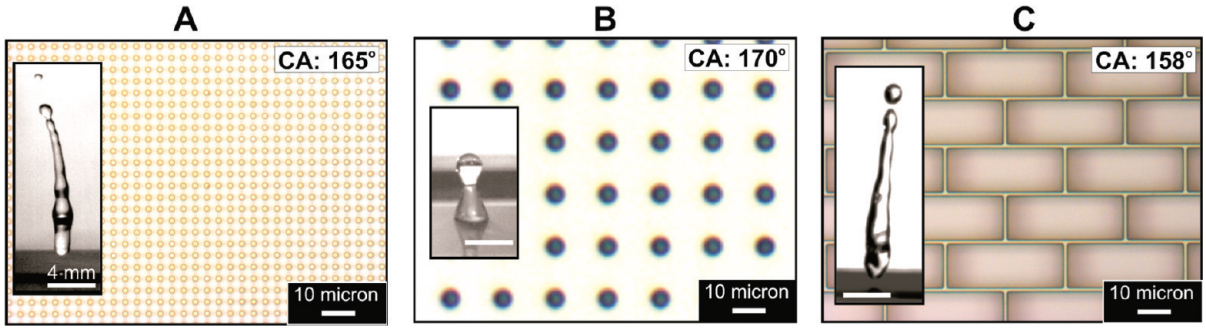

Figure 8. Optical images of open-cell nanopost structures (A, B) and a closed-cell brick structure (C) taken normal to the surface. Insets show dynamic retraction behavior of ~15 μL droplets impacting from a 10 cm height at room temperature conditions. Posts with small spacing (A) and bricks (C) remain superhydrophobic and repel the droplets, while posts with larger spacing show low pressure stability and fail upon droplet impact, leading to wetting (B). CA indicates the approximate value of the advancing contact angle formed by a droplet on the substrate.

transition substrate temperature wherein the retraction force reaches zero exactly at the end of droplet retraction. For temperatures lower than this transition temperature, the retraction force reaches zero before the droplet fully retracts, the contact line pins at that location, and the droplet eventually freezes (Figure 6F). Our model predicts the pinning transition temperature to be approximately −20 °C, in excellent quantitative agreement with the experimental results. The accuracy of the model hinges on the engineering precision and highly ordered nature of our surfaces.

This new insight into the mechanism and surface-dependence of dynamic freezing allows the above analysis to highlight some of the important factors that make *ordered* superhydrophobic surfaces an especially promising model system for developing effective, icephobic materials designs. First, pattern uniformity avoids surface inhomogeneities typical of disordered SHSs that would invariably induce uncontrolled local pinning and freezing of impacting droplets. This feature also allows for future detailed studies of heterogeneous nucleation and possible failure of these coatings. Second, one may consider the possibility of designing anisotropic surface geometries with direction-dependent wetting and dewetting characteristics,[25,26] (*e.g.*, we observed that ice accumulation on a SHS bearing an array of blades depends on the substrate orientation). Third, the ability to precisely engineer the contact surface topography suggests a means for controlling heat transfer from the droplet to the surface, potentially reducing the freezing temperature or increasing induction time for nucleation. Indeed, we have observed a significant delay in nucleation of nonwetting droplets on a SHS (Figure 7, Supporting Information, video 3), in agreement with a recent report.[22] Three droplets—one suspended (Cassie) droplet on the SHS region, one droplet on a flat hydrophobic region, and one partially wetting (partial Wenzel) droplet on the SHS region—were placed on the same silicon substrate and the temperature of the substrate was gradually decreased from 0 to −20 °C at a rate of −5 °C/min. All three droplets froze under the same substrate temperature (±1 °C) during this ramp, with a 16 s time delay between the first and last freezing events.

Another (and arguably most important) consideration for the design of icephobic materials is high hydrostatic and dynamic pressure stability—the maximum liquid pressure at which a surface can maintain superhydrophobic properties—as a droplet/surface collision may induce the transition from the nonwetting to the wetting state, increasing its adhesion in the event of freezing of the pinned droplet. The pressure stability for closed-cell geometries (such as bricks or honeycombs) is significantly higher than that of open-cell structures (such as posts) due to the confinement of air underneath the droplet in closed wells.[27] For example, we show that a SHS bearing a brick wall with features of 15 × 39 μm^2 (CA = 158°) effectively repels water droplets dropped from a 10 cm height, while an array of posts fails at half that feature spacing, though the latter surface shows even better static superhydrophobicity (CA = 170 °C) (Figure 8). Experiments carried out in a high-pressure test chamber show that a water droplet on closed-cell structures does not undergo any change in the contact angle even at pressures up to 40−60 atm. This implies that such surfaces should be able to retain superhydrophobicity upon impact with droplets traveling at 90−135 m/s (200−300 miles/h). These preliminary findings highlight the vastly superior pressure stability of closed-cell structures and make them ideal for developing stable, liquid-repelling surfaces for high-speed impact conditions.

Closed-cell geometries are not only favorable in terms of pressure stability, however. The ability to use larger feature sizes and continuity of the entire wall structure renders them more mechanically robust and amenable to facile replication by soft lithography[28] and imprinting.[29] Replication directly from a hydrophobic polymer could even obviate the need for additional hydrophobic chemical coatings and their subsequent degradation. Polymeric replicas of our brick and honeycomb samples, formed *via* soft lithography, demonstrated the same ice-repellent capabilities as the original silicon structures.

CONCLUSIONS

We have presented a comprehensive experimental and theoretical study of dynamic droplet freezing on structured surfaces by analyzing a broad range of geometries, impact angles, and droplet temperatures and comparing how wetting behavior on hydrophilic, hydrophobic, and superhydrophobic surfaces changes with supercooling. For the first time, the properties and geometry of superhydrophobic surfaces, surface−liquid interactions, droplet dynamics, ice nucleation, and ice prevention have been integrated into one unified picture. The investigation revealed a novel mechanism highlighting the importance of dynamic wetting behavior that leads to full retraction and repulsion of impacting water droplets from a cooled SHS *before* ice nucleation occurs. Owing to a unique *nonwetting* freezing transition appearing at −25 to −30 °C, ice accumulated below this temperature can be easily removed, while ice formation is *fully prevented* above this transition. This level of systematic study, previously unachieved with other systems, showed the high promise of nano- and microstructured SHSs as anti-icing materials and allowed us to provide several guiding principles for the development of this model system into a scalable, rationally designed, ice-preventive technology that requires no (or minimal) active energy inputs. In particular, we emphasize the potential of hydrophobic polymeric coatings bearing closed-cell surface microstructures for their improved mechanical and pressure stability, amenability to facile replication, large-scale fabrication, and opportunities for greater tuning of their material and chemical properties.

We believe that this work provides a solid foundation for a radical and much-needed shift in icephobic technological strategies: complete prevention of ice nucleation *via* droplet deflection by stable, built-in surfaces that remain continuously ice-free at significant supercooling. The identification of the deflection mechanism and our predictive model, synthesizing this mechanism with a set of critical parameters, provide a comprehensive framework for optimizing robust superhydrophobic surfaces for a wide range of applications.

METHODS

Ice accumulation studies were performed on structured and unstructured surfaces under conditions of dynamic flow of water onto the test substrates (Figure 9). Water droplets at room temperature (RT), 60 °C, 0 °C or supercooled to −5 °C, were dropped onto substrates (F) kept at controlled temperatures (−35 °C to RT), and positioned at fixed angles (β) of 0°, 30°, and 60° to the horizontal. The experimental setup involves a capillary tube (C) in contact with a thermoelectric cooler (B, TE Technology CP-065) and temperature controller (A, TC-48-20) mounted above a closed desiccator chamber (L, Secador). Water droplets are formed at the tip of a temperature-controlled capillary tube and fall onto a sample substrate positioned at a controlled distance (10 cm) below. (Note: Droplet temperature does not significantly change during the short time-of-flight, although the air inside the chamber was not actively cooled.) The samples are mounted onto a thermoelectric cooling stage (G and H, Instec TS62) attached to an angled micromanipulator stage (M, World Precision Instruments), controlled remotely outside the chamber. An air flow (K) was used to keep the environment in the desiccator chamber dry (~5% humidity) and reduce condensation on the substrates. A syringe pump (E, Kd Scientific) was used to control the water flow to the capillary through flexible tubing (D). The schematic also shows part of the optical imaging system (I) used to capture (through a viewing window J) the motion and ice residue of the droplets as they impact the substrates. The imaging system consisted of a long working distance macro lens (Canon 28, 135 mm), an aperture-controlling lens adapter ring (Birger Engineering) and a high-resolution color still image (Canon EOS 40D) or high-speed video camera (Phantom V7.3, 10000 fps).

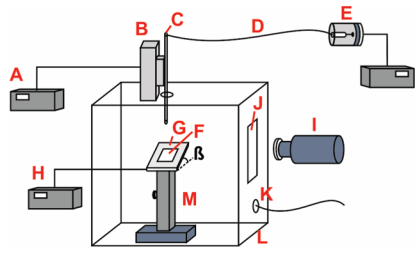

Figure 9. Schematic of the experimental setup.

The array of silicon nanostructures presented in this work (Table 1) was fabricated using the Bosch process, as described elsewhere.[10] The nanostructured silicon surfaces were treated with a hydrophobic silane (tridecafluoro-1,1,2,2-tetrahydrooctyl)-trichlorosilane (Gelest Inc.) by vapor exposure in a desiccator under vacuum overnight. Table 2 describes the wetting properties of the smooth hydrophobic silicon surface (treated with the same vapor silane method as above) and post and brick arrays used in the experiments.

Acknowledgment. We would like to thank L. Stirling and A. Grinthal for their valuable contribution. This work was funded in part by DARPA (Award Number HR0011-08-C-0114) and the Wyss Institute for Biologically Inspired Engineering. L. Mishchenko thanks the U.S. Department of Homeland Security (DHS) Scholarship and Fellowship Program for financial support.

Supporting Information Available: Three videos showing dynamic behavior of single droplets impinging upon tilted surfaces below 0 °C, removal of droplets frozen on smooth hydrophobic and superhydrophobic surfaces, and freezing of static droplets on smooth hydrophobic silicon and superhydrophobic silicon. This material is available free of charge *via* the Internet at http://pubs.acs.org.

REFERENCES AND NOTES

1. Gent, R. W.; Dart, N. P.; Cansdale, J. T. Aircraft Icing. *Philos. Trans R. Soc., A* **2000**, *358*, 2873–2911.
2. Gao, X. F.; Yan, X.; Yao, X.; Xu, L.; Zhang, K.; Zhang, J. H.; Yang, B.; Jiang, L. The Dry-Style Antifogging Properties of Mosquito Compound Eyes and Artificial Analogues Prepared by Soft Lithography. *Adv. Mater.* **2007**, *19*, 2213–2217.
3. Gao, X. F.; Jiang, L. Water-Repellent Legs of Water Striders. *Nature* **2004**, *432*, 36.
4. Autumn, K.; Liang, Y. A.; Hsieh, S. T.; Zesch, W.; Chan, W. P.; Kenny, T. W.; Fearing, R.; Full, R. J. Adhesive Force of a Single Gecko Foot-Hair. *Nature* **2000**, *405*, 681–685.

5. Zheng, Y. M.; Gao, X. F.; Jiang, L. Directional Adhesion of Superhydrophobic Butterfly Wings. *Soft Matter* **2007**, *3*, 178–182.
6. Patankar, N. A. Mimicking the Lotus Effect: Influence of Double Roughness Structures and Slender Pillars. *Langmuir* **2004**, *20*, 8209–8213.
7. Varanasi, K. K.; Hsu, M.; Bhate, N.; Yang, W. S.; Deng, T. Spatial Control in the Heterogeneous Nucleation of Water. *Appl. Phys. Lett.* **2009**, *95* (1−3), 094101.
8. Gavish, M.; Popovitzbiro, R.; Lahav, M.; Leiserowitz, L. Ice Nucleation by Alcohols Arranged in Monolayers at the Surface of Water Drops. *Science* **1990**, *250*, 973–975.
9. Ehre, D.; Lavert, E.; Lahav, M.; Lubomirsky, I. Water Freezes Differently on Positively and Negatively Charged Surfaces of Pyroelectric Materials. *Science* **2010**, *327*, 672–675.
10. Krupenkin, T. N.; Taylor, J. A.; Wang, E. N.; Kolodner, P.; Hodes, M.; Salamon, T. R. Reversible Wetting−Dewetting Transitions on Electrically Tunable Superhydrophobic Nanostructured Surfaces. *Langmuir* **2007**, *23*, 9128–9133.
11. Ahuja, A.; Taylor, J. A.; Lifton, V.; Sidorenko, A. A.; Salamon, T. R.; Lobaton, E. J.; Kolodner, P.; Krupenkin, T. N. Nanonails: A Simple Geometrical Approach to Electrically Tunable Superlyophobic Surfaces. *Langmuir* **2008**, *24*, 9–14.
12. Tuteja, A.; Choi, W.; Ma, M. L.; Mabry, J. M.; Mazzella, S. A.; Rutledge, G. C.; McKinley, G. H.; Cohen, R. E. Designing Superoleophobic Surfaces. *Science* **2007**, *318*, 1618–1622.
13. Roach, P.; Shirtcliffe, N. J.; Newton, M. I. Progess in Superhydrophobic Surface Development. *Soft Matter* **2008**, *4*, 224–240.
14. Li, X. M.; Reinhoudt, D.; Crego-Calama, M. What Do We Need for a Superhydrophobic Surface? A Review on the Recent Progress in the Preparation of Superhydrophobic Surfaces. *Chem. Soc. Rev.* **2007**, *36*, 1350–1368.
15. Patankar, N. A. Transition between Superhydrophobic States on Rough Surfaces. *Langmuir* **2004**, *20*, 7097–7102.
16. Bird, J. C.; Mandre, S.; Stone, H. A. Short-Time Dynamics of Partial Wetting. *Phys. Rev. Lett.* **2008**, *100* (1−4), 234501.
17. Richard, D.; Clanet, C.; Quere, D. Surface Phenomena−Contact Time of a Bouncing Drop. *Nature* **2002**, *417*, 811.
18. Deng, T.; Varanasi, K. K.; Hsu, M.; Bhate, N.; Keimel, C.; Stein, J.; Blohm, M. Nonwetting of Impinging Droplets on Textured Surfaces. *Appl. Phys. Lett.* **2009**, *94*, 133109.
19. Jung, Y. C.; Bhushan, B. Dynamic Effects of Bouncing Water Droplets on Superhydrophobic Surfaces. *Langmuir* **2008**, *24*, 6262–6269.
20. Kulinich, S. A.; Farzaneh, M. How Wetting Hysteresis Influences Ice Adhesion Strength on Superhydrophobic Surfaces. *Langmuir* **2009**, *25*, 8854–8856.
21. Sarkar, D. K.; Farzaneh, M. Superhydrophobic Coatings with Reduced Ice Adhesion. *J. Adhes. Sci. Technol.* **2009**, *23*, 1215–1237.
22. Tourkine, P.; Le Merrer, M.; Quere, D. Delayed Freezing on Water Repellent Materials. *Langmuir* **2009**, *25*, 7214–7216.
23. Cao, L. L.; Jones, A. K.; Sikka, V. K.; Wu, J. Z.; Gao, D. Anti-icing Superhydrophobic Coatings. *Langmuir* **2009**, *25*, 12444–12448.
24. He, M.; Wang, J. X.; Li, H. L.; Jin, X. L.; Wang, J. J.; Liu, B. Q.; Song, Y. L. Super-Hydrophobic Film Retards Frost Formation. *Soft Matter* **2010**, *6*, 2396–2399.
25. Chu, K. H.; Xiao, R.; Wang, E. N. Unidirectional Liquid Spreading on Asymmetric Nanostructured Surfaces. *Nat. Mater.* **2010**, *9*, 413–417.
26. Yoshimitsu, Z.; Nakajima, A.; Watanabe, T.; Hashimoto, K. Effects of Surface Structure on the Hydrophobicity and Sliding Behavior of Water Droplets. *Langmuir* **2002**, *18*, 5818–5822.
27. Bahadur, V.; Garimella, S. V. Preventing the Cassie−Wenzel Transition Using Surfaces with Noncommunicating Roughness Elements. *Langmuir* **2009**, *25*, 4815–4820.
28. Pokroy, B.; Epstein, A. K.; Persson-Gulda, M. C. M.; Aizenberg, J. Fabrication of Bioinspired Actuated Nanostructures with Arbitrary Geometry and Stiffness. *Adv. Mater.* **2009**, *21*, 463–469.
29. Gates, B. D.; Xu, Q. B.; Stewart, M.; Ryan, D.; Willson, C. G.; Whitesides, G. M. New Approaches to Nanofabrication: Molding, Printing, and Other Techniques. *Chem. Rev.* **2005**, *105*, 1171–1196.